THE JOURNAL OF PHYSICAL CHEMISTRY B
A JOURNAL OF THE AMERICAN CHEMICAL SOCIETY

pubs.acs.org/JPCB

Article

Hypergolicity of Cyanoborohydride Ionic Liquids with H_2O_2 and HNO_3 as Oxidizers in the Liquid Phase

Komal Yadav, Ralf Kaiser, and Rui Sun*

Cite This: *J. Phys. Chem. B* 2025, 129, 13258−13266

Read Online

ACCESS | Metrics & More | Article Recommendations | Supporting Information

ABSTRACT: Ab initio molecular dynamics simulations were performed to investigate the reaction mechanisms and kinetics of the ionic liquid 1-ethyl-3-methylimidazolium cyanoborohydride ($[EMIM]^+[CBH]^-$) with two oxidizers, hydrogen peroxide (H_2O_2) and nitric acid (HNO_3), in liquid phases. Neither of the systems is unstable enough to react within the time frame of unbiased simulations; thus, well-tempered metadynamics was employed to accelerate reactions along selected collective variables (CVs). A large number of CVs were screened, and the CVs corresponding to the lowest bias energy were chosen. The required bias energy for oxidation of the $[EMIM]^+[CBH]^-/H_2O_2$ system was found to be about half of what is required for $[EMIM]^+[CBH]^-/HNO_3$. Reaction rate constants estimated using infrequent metadynamics indicate that the oxidation with H_2O_2 is about 10^{10} times faster than that with HNO_3. Both results agree with the levitated droplet merging experiments, which showed that rock-grade H_2O_2 is a much more efficient oxidizer. Analysis of the trajectories reveals an extensive rearrangement of the hydrogen bond network in the H_2O_2 system.

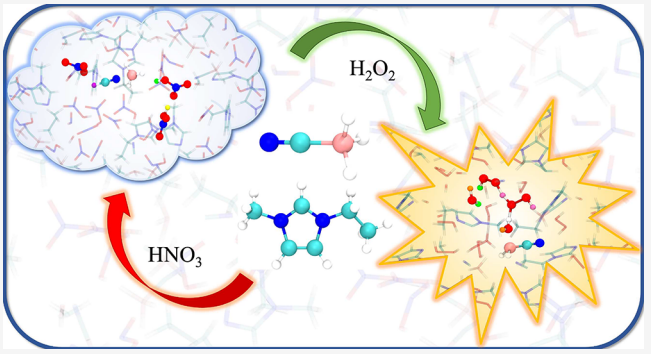

INTRODUCTION

Hypergolic bipropellants stand as a crucial element in aerospace endeavors, serving as the elemental force that propels rockets, missiles, and spacecrafts to the farthest reaches of our exploration.[1] Compared with traditional fuels, hypergolic bipropellants do not require a separate ignition system, thus reducing the complexity and potential failure points of the engine. However, the most commonly adopted hypergolic bipropellants, hydrazine (N_2H_4) and its derivatives (as fuels), along with nitrogen tetroxide (N_2O_4, as oxidizers), are extremely corrosive, toxic, and carcinogenic.[1,2] As a result, there is growing interest in alternative hypergolic bipropellant options that offer improved safety and environmental friendliness. In recent years, hypergolic ionic liquid (HIL) based bipropellants have emerged as a new class of fuels offering environmental friendliness, low toxicity, ease of handling, and extremely low vapor pressure.[3−5] The first synthesis of HILs, 1-allyl-3-methylimidazolium dicyanamide with an oxidizer (red or white fuming nitric acid) by Schneider et al. in 2008, marks a pivotal shift towards green propellants.[6] Since then, a wide variety of ionic liquids have been synthesized and evaluated for their potential as HILs. These include a range of cations based on triazolium, imidazolium, and tetrazolium frameworks, combined with anions such as nitrocyanamide and dicyanamide, and paired with oxidizers like red or white fuming nitric acid (HNO_3) and high-concentration hydrogen peroxide (H_2O_2 above 90% rocket grade).[7−11] Comprehensive experimental and computational studies have further explored ideal HIL candidates, underscoring their transformative potential as eco-friendly hypergolic bipropellants.

Among these, cyanoborohydride-based ionic liquids are emerging as promising candidates. Specifically, 1-ethyl-3-methylimidazolium cyanoborohydride ($[EMIM]^+[CBH]^-$) undergoes a hypergolic reaction with short ignition delay[6] when contacting white fuming nitric acid (WFNA).[12−16] First reported by Zhang et al. in 2011, $[EMIM]^+[CBH]^-$ is thermally stable, moisture-resistant, and offers high energy density due to its boron-centered anion, $[BH_3(CN)]^-$, making it an ideal HIL candidate.[13] However, the hypergolicity and ignition delay[7] were measured using the conventional drop test in which a submilliliter-sized droplet is allowed to fall in a pool of oxidizer (usually a few to tens of milliliters). The ignition delay was extracted from images captured with a millisecond temporal resolution. However, the lack of well-defined experimental parameters in the drop tests may have led to substantial misinterpretation of $[EMIM]^+[CBH]^-$ hypergolicity with certain oxidizers.[12−20] For example, conducted in air, the drop test does not rule out the potential role that

Received: October 21, 2025
Revised: December 3, 2025
Accepted: December 4, 2025
Published: December 11, 2025

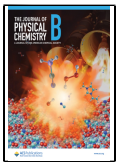

https://doi.org/10.1021/acs.jpcb.5c07210
J. Phys. Chem. B 2025, 129, 13258−13266

molecular oxygen (O_2) might play in the hypergolic ignition. In addition, it remains unclear whether the overwhelmingly excessive amount of the oxidizer plays a role.

In this regard, Kaiser and co-workers recently studied the ignition chemistry of $[EMIM]^+[CBH]^-$ with different concentrations of WFNA under controlled experimental conditions.[21] Their experiment highlights a closed process chamber where acoustically levitated droplets of ionic liquid and droplets of the oxidizer are merged, and the consequential chemical reactions were characterized by complementary in situ diagnostics - infrared (IR), Raman (Ra), ultraviolet−visible (UV−vis) spectroscopy, and VIS/IR thermal imaging. When the chamber is filled with inert (Ar) gas, merging of the $[EMIM]^+[CBH]^-$ droplet with the WFNA droplet results in gas-phase products (e.g., N_2O, HCN, and NO_2), but there is no ignition. Interestingly, the reaction system becomes hypergolic if the O_2 gas is also included in the chamber. Computational study reveals that O_2 can react with a key reactive intermediate (e.g., N-boryl-N-oxo-formamide) formed after the merging of the droplets.[22] The oxidized intermediate can further degrade into BO_2, H_2O, $BH(OH)_2$, and HCONOH in highly exothermic reactions, thus triggering ignition. Hydrogen peroxide (H_2O_2) is another commonly used oxidizer in hypergolic bipropellants.[23−27] Compared to WFNA, H_2O_2 features its environmentally friendly combustion products, low vapor pressure, high density, and ease of handling.[28] Kaiser and co-workers also investigated the merging of the $[EMIM]^+[CBH]^-$ droplet with the H_2O_2 droplet.[22] The results show that even in an inert (Ar) environment, as long as H_2O_2 is over 80% w/v, ignition occurs within a few microseconds after merging and is followed by a violent reaction that forms small molecules like HCN, BO_2, and H_2O. These experiments provide compelling evidence that hypergolicity is oxidizer-dependent and that the reaction mechanisms are sensitive to experimental parameters such as the relative ratio between $[EMIM]^+[CBH]^-$ and the oxidizer, as well as the presence of O_2 in the process chamber.

The potential energy surface (PES) of the oxidation of hypergolic ionic liquids has been studied extensively[21,22,29−32] and an overwhelming majority of these studies have been conducted in the gas phase. The details of the PESs vary from one reaction system to another, but the following three steps are in common: (1) exothermic associations between the hypergolic ionic liquid (usually just the anion) and the oxidizer to form van der Waals complexes, (2) extensive isomerization of the hydrogen-bond complexes with nonsubmerged barrier(s) to covalent complexes, and (3) releasing the chemical energies stored in the covalent bonds and dissociating into gas phase products. Step (2) usually corresponds to proton or hydroxyl (·OH) transfer from the oxidizer to the anion of the ionic liquid and is the rate-limiting step. Therefore, the highest barrier in Step (2) has been employed to predict whether a certain combination of an ionic liquid and oxidizer is hypergolic.

One potential issue of these gas-phase PES studies is that the barriers in Step (2) always seem to be too high for hypergolic ignition.[33−35] For example, barriers in this step are over 20 kcal/mol in the gas phase PES reported by Liu and co-workers for the reaction of NO_2 with three different imidazolium cations (1-ethyl-3-methylimidazolium dicyanamide, 1-butyl-3-methylimidazolium dicyanamide, and 1-allyl-3-methylimidazolium dicyanamide) and with 1-methyl-4-amino-1,2,4-triazolium dicyanamide.[30] These values are more than 1 order of magnitude higher than the energy range of thermal fluctuation; thus, it is difficult to comprehend that reactions possessing such barriers could take place on the time scale of a microsecond (i.e., the time scale of ignition delay in hypergolic bipropellant). As such, those PESs should be considered only qualitatively in predicting hypergolicity.

Calculations with implicit solvents were also carried out to account for the reaction in the condensed phase. However, implicit solvents could misrepresent the entropic effect of the reaction and, more importantly, oversimply the hydrogen-bond network in the liquid phase (e.g., the Grotthuss mechanism). These problems could lead to an overestimation of the barriers in Step (2). Take the $[CBH]^-$ + HNO_3 system as an example, Fujioka et al. showed that the gas phase transition state barrier for the proton transfer decreases by over 30.0 kcal/mol when the system has one additional HNO_3 molecule.[36] This is also true with H_2O_2 as the oxidizer, where they found that the barrier in Step (2) is entirely submerged if there are two H_2O_2 in the system, as compared to having a barrier of ∼8 kcal/mol when only one H_2O_2 is used to compute the gas phase PES.[22] Liu et al. also reported the same phenomena in the reaction modeling of nitric acid oxidation of dicyanoborohydride and dicyanamide anions. They observed that the addition of the second HNO_3 to the reaction profile not only lowers the reaction barrier and stabilizes the intermediates (by more than tens of kcal/mol) but also leads to the barrierless formation of two exothermic products.[34]

This article aims to characterize the rate-limiting step of the oxidation of hypergolic ionic liquid with quantum chemistry calculations and dynamics simulations in the liquid phase. Two oxidizers, HNO_3 and H_2O_2, are employed to react with $[EMIM]^+[CBH]^-$, where only the latter oxidizer is shown to be hypergolic by experiments. We aim to understand the factors contributing to the hypergolic nature of one oxidizer over the other.

METHODS

We prepared a cubic box containing 5 $[EMIM]^+[CBH]^-$ pairs and 20 oxidizer molecules (H_2O_2/HNO_3) using PACKMOL (see Figure 1).[37] We used a 1:4 molar ratio of $[EMIM]^+[CBH]^-$ to H_2O_2 since experimentally the hypergolic ignition was observed only at or above this ratio.[22] The system first goes through energy minimization and then equilibration

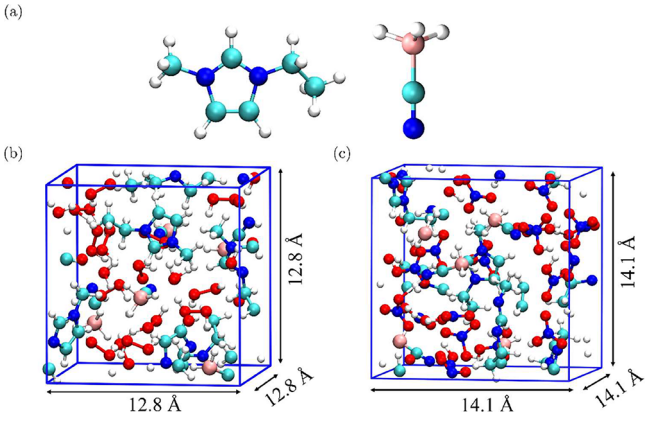

Figure 1. (a) Structures of the ionic liquid pair $[EMIM]^+[CBH]^-$ and the boxes with equilibrated box lengths containing (b) $[EMIM]^+[CBH]^-$ + H_2O_2 and (c) $[EMIM]^+[CBH]^-$ + HNO_3.

https://doi.org/10.1021/acs.jpcb.5c07210
J. Phys. Chem. B 2025, 129, 13258−13266

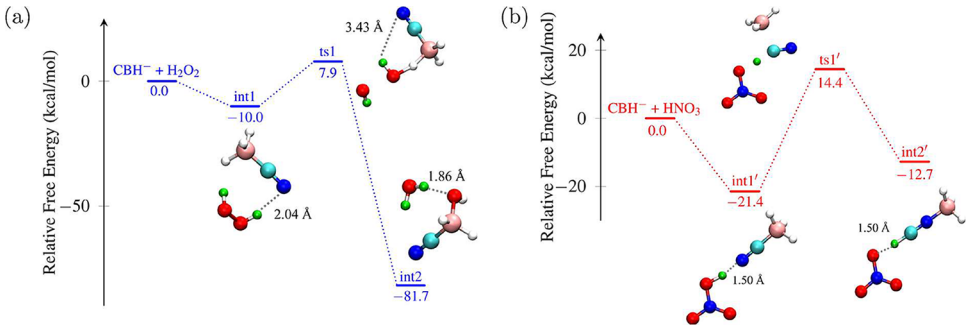

Figure 2. Free energy profiles for the initial decomposition steps of (a) CBH^- + H_2O_2 and (b) CBH^- + HNO_3 systems calculated at a temperature of 298.15 K.

using all-atom classical molecular dynamics simulations, where the potentials are modeled using the generalized Amber force fields,[38] using the CP2K[39] software. Next, we perform a constant NPT (298.15 K and 1 bar) simulation to ensure the proper system density. We then equilibrate the system isotropically again with constant NPT with ab initio molecular dynamics (AIMD) simulations using the barostat developed by Martyna et al.,[40] to maintain a proper density (∼1.1 g/cm^3). Finally, we equilibrate the box at a constant NVT ensemble using the CSVR (canonical sampling through velocity rescaling)[41] thermostat to generate configurations for the production runs.

Choosing an appropriate level of theory that balances the computational cost and accuracy is key to successful dynamics simulations of the $[EMIM]^+[CBH]^-$ + HNO_3/H_2O_2 system in the condensed phase. All AIMD simulations are performed with the BLYP functional[42,43] and a TZV2P basis set.[44] The Goedecker-Teter-Hutter (GTH) pseudopotentials[45] describe the interactions between the ionic cores and valence electrons. We employ the hybrid Gaussian and Plane-waves method (GPW)[46] with the Quickstep module in CP2K, which uses the atom-centered Gaussian-type orbitals to describe the wave function and an auxiliary plane wave basis set for expansion of the electron density. This same level of theory is employed for simulations of chemical reactions in room temperature ionic liquid of similar sizes,[47,48] where careful benchmarking was performed against functional of higher hierarchy and larger basis sets. We set a plane wave cutoff of 450 Ry and employ Grimme's dispersion correction (DFT-D3)[49] to treat the long-range van der Waals interaction. The equations of motion are integrated with a 0.5 fs time step. For each system ($[EMIM]^+[CBH]^-$ + HNO_3/H_2O_2), 50 frames are obtained from AIMD NVT simulations, from which we initiate well-tempered metadynamics (WTMetaD)[50] simulations with the PLUMED plug-in.[50] The parameters employed by WTMetaD and the collective variables used will be explained in the Results section. Our simulation setup and parameters employed for the condensed phase simulations are largely inspired by recent work on chemical reactions in room-temperature ionic liquids by Voth and co-workers.[4748]

RESULTS AND DISCUSSION

Reactions in the Gas Phase. For the gas phase calculations, we follow the experimental finding that the anion primarily influences the chemical properties of ionic liquid systems and focus on the reaction between the anion and the oxidizer molecule.[6,12,51−53] We use the Becke, Lee−Yang−Parr (BLYP) functional[42,43] with 6-31G(d)[44,54] basis set, and Grimme's D3[49] dispersion correction for the gas phase PES calculation. This level of theory is low, but it is chosen because it agrees well with the reference PES,[36] as well as closely resembles the level of theory used in the liquid phase AIMD simulations. This consistency is important to relate the condensed phase reaction dynamics to the gas phase reaction. We follow the intrinsic reaction coordinate (IRC)[55] in both directions of the transition state to connect to its respective intermediates.

The initial steps of the reaction for both systems follow what was reported by Fujioka et al.,[22,36] and their free energy profiles (at 298.15 K) are shown in Figure 2. In the case of H_2O_2, a H-bond complex (**int1**, N--H distance: 2.04 Å) forms with the N-terminal of CBH^-, weakening the O−O bond. The oxidizer then dissociates into two ·OH radicals, where one associates with the -BH_3 terminal of CBH^- (**ts1**). This step is the rate-limiting step for ignition, and its energy is ∼17.9 kcal/mol above stable hydrogen-bonded complex **int1**. The hydrogen in the ·OH radical of **ts1** eventually transfers back to the other ·OH radical and forms H_2O. Simultaneously, the OH group attached to boron tumbles to form a B−O bond (**int2**). **int2** is stabilized by a hydrogen bond between the $H_2B(OH)$ moiety and H_2O (O--H distance: 1.86 Å). Overall, in the process of forming **int2** from the separated reactants, one oxygen atom from H_2O_2 inserts into the B−H bond of CBH^- and releases some 81.7 kcal/mol energy.

When HNO_3 is the oxidizer, the association of the reactants forms a hydrogen bond between the H atom of HNO_3 and the N atom of CBH^- (**int1'**, N--H bond distance: 1.50 Å). The proton transfer from HNO_3 to CBH^- takes place via a concerted three-membered ring (involving B, C, and N atoms) transition state, **ts1'**. This step involves a simultaneous isomerization (from H_3BCN to H_3BNC) and a proton transfer from HNO_3 to the C-terminal of H_3BNC, leading to the formation of **int2'**. **int2'** is a H-bond complex (O--H bond distance: 1.50 Å) between H_3B-NCH and NO_3^-. **ts1'** was reported to be the rate-limiting step of the oxidation of CBH^- with HNO_3 by Fujioka et al.,[22,36] and is ∼35.8 kcal/mol above the hydrogen-bonded complex **int1'** in this study. Overall, forming **int2'** involves a proton transfer from the oxidizer and the rotation of the cyano group in CBH^-, and it is exothermic, releasing 12.7 kcal/mol energy.

The free energy profile of both reactions qualitatively supports the findings of the levitated droplet experiments[21,22] in the sense that (1) temperature rising after droplet merging (e.g., forming **int1** and **int1'** is exothermic) and (2) H_2O_2 is more reactive than HNO_3 as an oxidizer (e.g., barrier height **ts1** < **ts1'**). It is also important to note qualitative differences

https://doi.org/10.1021/acs.jpcb.5c07210
J. Phys. Chem. B 2025, 129, 13258−13266

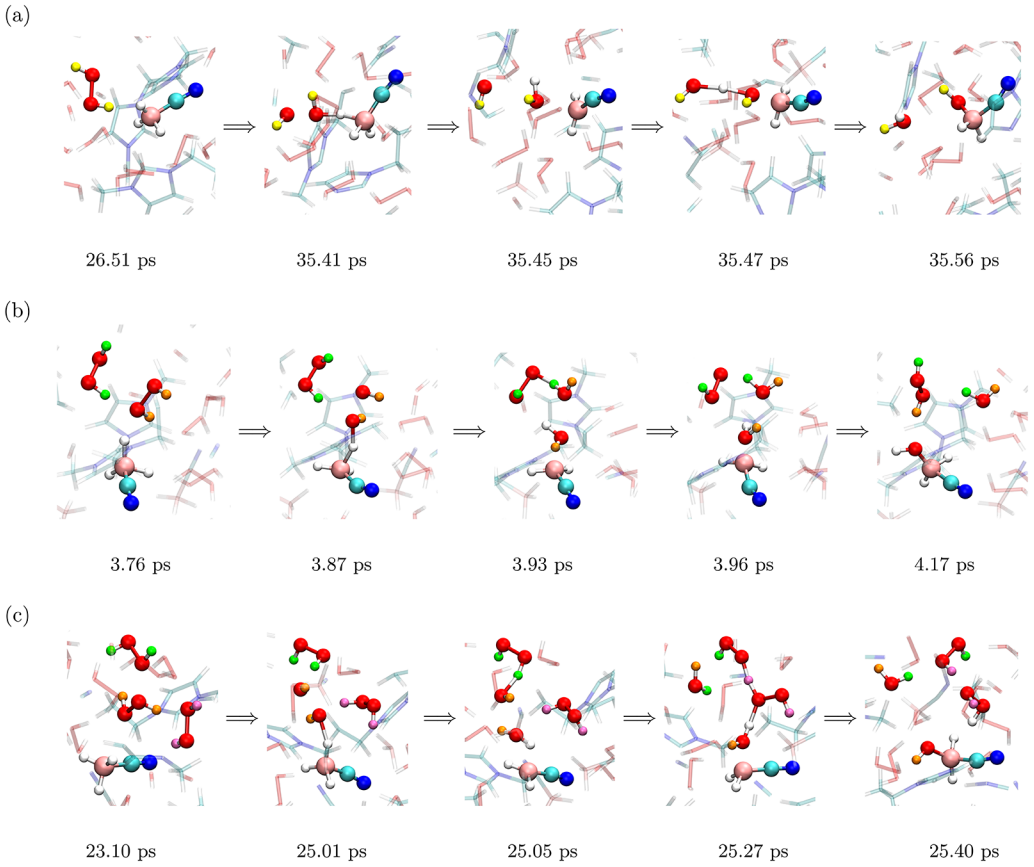

Figure 3. Snapshots of trajectories showing the reaction between CBH^- and H_2O_2 where the proton abstraction to form $H_3B(OH)CN^-$ involves (a) one H_2O_2, (b) two H_2O_2, and (c) three H_2O_2 molecules.

between the free energy profile (Figure 2) and the levitated droplet experiments. The barrier of the reaction (17.9 kcal/mol for H_2O_2 and 35.8 kcal/mol for HNO_3) is too high for reactions to be spontaneous, let alone hypergolic. Studies employing higher-level theories (e.g., Fujioka et al.[22,36]) reported very similar barrier height.

Reactions in the Liquid Phase: $[EMIM]^+/[CBH]^-$ + H_2O_2. Instead of assuming that the reaction follows the initial steps as indicated in the gas phase (Figure 2), the first goal is to explore whether the system is inherently unstable enough to be reactive in the liquid phase. Unbiased AIMD simulations are carried out with the NVT ensemble at 298.15 K for a total of 20 ps. No chemical reactions are observed within this time frame. Well-tempered metadynamics (WTMetaD) is then applied to both systems to accelerate the reaction. WTMetaD adds a time-dependent bias energy to the Hamiltonian of the system along the collective variables (CVs). This energy pushes the system out of free energy minima and lets it explore configurational spaces not accessed by the unbiased simulations. The CVs are selected to capture the configurational change of the rate-limiting step, as shown in the gas-phase reaction (Figure 2). For the $[EMIM]^+[CBH]^-$ + H_2O_2 system, the targeted pathway (**int1** → **ts1** → **int2**) involves the simultaneous dissociation of the O−O bond and the formation of the B−H-−O-H hydrogen bond. We randomly selected one CBH anion as the reactive molecule, which can react with all H_2O_2 molecules in the system. A combination of two CVs is chosen: CV1 is the coordination number between all three hydrogen atoms in $-BH_3$ and the oxygen atom from all H_2O_2 molecules; CV2 is the coordination number between boron and the three hydrogen atoms in $-BH_3$. The two CVs are shown in Figure S1 in the ESI. As the system progresses from **int1** to **int2**, one B−H bond dissociates, and the dissociated hydrogen forms a new bond with a hydroxyl radical (·OH) resulting from H_2O_2 dissociation; i.e., CV2 decreases and CV1 increases.

Independent WTMetaD simulations with constant NVT are initiated from 50 different frames chosen randomly from the unbiased simulation. A Gaussian bias is deposited every 50 steps with a height of 0.5 kcal/mol and a width of 0.1 for both CVs. The simulations stop once a chemical reaction is observed. As such, the bias energy from WTMetaD accelerates the reaction by disturbing the system in a controlled manner instead of its traditional role of estimating the free energy of the reaction. This choice is made for two reasons: (1) The goal of the research is to understand why the hypergolicity of $[EMIM]^+[CBH]^-$ is oxidizer dependent. As mentioned in the Introduction, the forward reaction (e.g., hydroxyl and proton transfer) is the rate-limiting step, after which the temperature of the system increases and triggers the decomposition. And (2) as it has been well-documented in reactions with extensive hydrogen bond network rearrangement, the backward reaction is extremely difficult to capture with enhanced sampling methods like WTMetaD.[56,57] Therefore, limited resources are dedicated to the forward reaction only.

The 50 independent WTMetaD simulations reveal that the reaction (**int1** → **int2**) is accompanied by an extensive hydrogen bond network rearrangement. Similar to the gas phase reaction, the reaction starts with one of the ·OH radicals (from the dissociation of the O−O bond in H_2O_2) abstracting

https://doi.org/10.1021/acs.jpcb.5c07210
J. Phys. Chem. B 2025, 129, 13258−13266

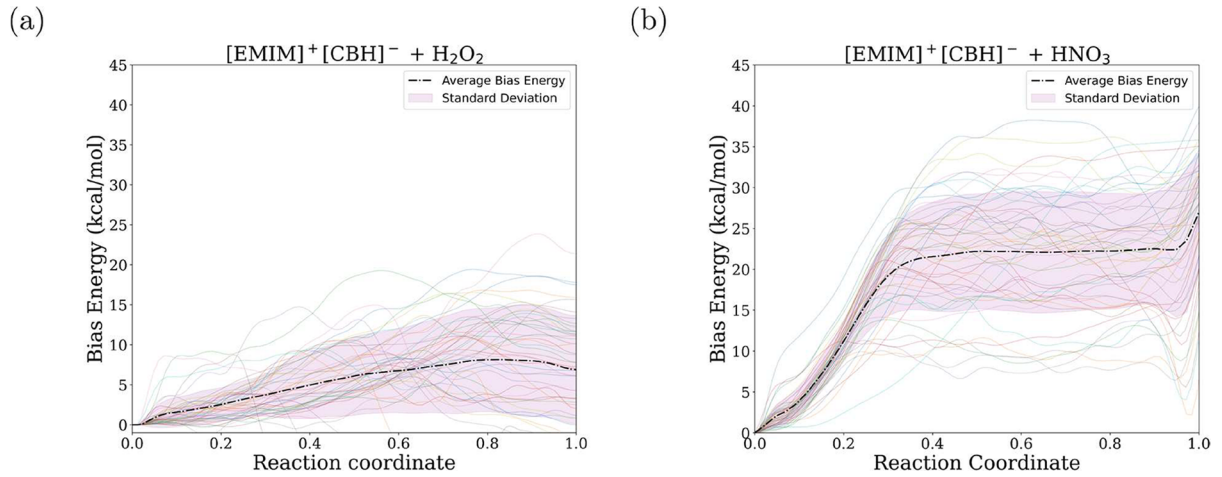

Figure 4. Bias energy profiles for all 50 WTMetaD trajectories for (a) IL+H_2O_2, and (b) IL+HNO_3 systems when a reaction takes place. The average bias energy along the reaction coordinate is plotted with a dotted-dashed black line.

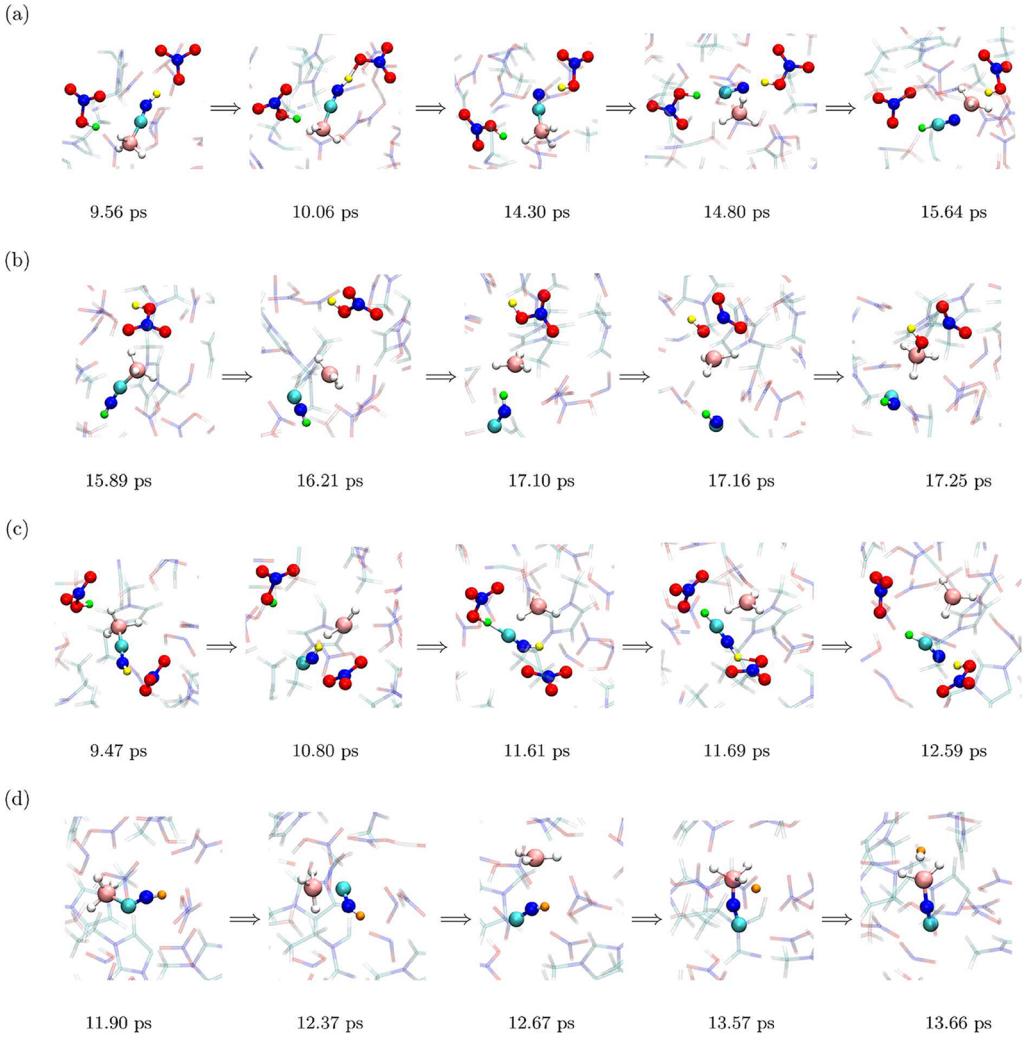

Figure 5. Snapshots of trajectories showing the reaction between CBH^- and HNO_3: (a) formation of HCN via **int2'**, (b) formation of HNC, (c) formation of HNC which later forms HCN via a proton transfer from a neighboring HNO_3 molecule, and (d) formation of H_2 molecules.

a hydrogen from the -BH_3 group in CBH^- and forms one H_2O molecule. In contrast to the gas phase reaction, where this newly formed H_2O molecule can undergo only a hydrogen bond exchange with the other adjacent ·OH radical to form $H_2B(OH)CN^-$ (**int2**), the hydrogen bond network surrounding the reactant can rearrange extensively. Snapshots from three example trajectories are shown in Figure 3, where one (Figure 3a), two (Figure 3b), and three (Figure 3c) different

https://doi.org/10.1021/acs.jpcb.5c07210
J. Phys. Chem. B 2025, 129, 13258−13266

H_2O_2 molecules can be involved in this process. As each trajectory starts from a different configuration, the bias energy needed for the reaction to occur is different. Figure 4a shows the barriers associated with the bias energy range from 5 to 20 kcal/mol, with the average value of ∼12 kcal/mol and a standard deviation of ∼4 kcal/mol. The bias energy reported in Figure 4a is obtained from the minimum energy path computed using the zero-temperature string method.[58]

It is important to note that biased MD simulations, such as WTMetaD, force the reaction to occur primarily along a path defined by the CVs. Since CVs are chosen prior to the simulations with chemical intuition, the reaction pathway found with a certain set of CVs is not necessarily the minimum free energy path. In addition to the aforementioned one (Figure S1a), multiple CVs that can promote the targeted reaction pathway (e.g., **int1** → **int2**) have been attempted, including singles and combinations of the coordination number between the boron and all oxygens from all H_2O_2 molecules, the B−C bond length, and the O−O bond length in a randomly selected H_2O_2 molecule. However, these CVs require a higher bias energy to induce the targeted or other reactions.

Reactions in the Liquid Phase: $[EMIM]^+/[CBH]^-$ + HNO_3. Similar to $[EMIM]^+[CBH]^-$ + H_2O_2, no oxidation reactions take place within the time frame of the unbiased simulations for $[EMIM]^+[CBH]^-$ + HNO_3. However, it is interesting to note that a proton spontaneously transfers from HNO_3 to CBH^- forming $[H_3BCN\text{-}H]$ and $[NO_3]^-$. Therefore, WTMetaD was employed to accelerate the target reaction. As shown in Figure 2b, the first step of the gas phase reaction features a rotation of the B−C group to form H_3B-NC, accompanied by a proton transfer from HNO_3 to form H_3BNCH (**int2'**) and $[NO_3]^-$. As argued for the $[EMIM]^+[CBH]^-$ + H_2O_2 reaction, different CVs (e.g., the B−C bond length, the coordination number between the carbon atom of CBH^- and the hydrogens of all HNO_3 molecules, the coordination number between all three hydrogens of -BH_3 and the oxygens of all HNO_3 molecules, and the bond angle ∠BCN) and their combinations have been attempted to accelerate the reaction. Several CVs are designed to weaken B−H bonds in the -BH_3 group with the hope of seeing if deprotonation of -BH_3 can trigger hydrogen network rearrangement and facilitate the target reaction. It turns out that the target reaction is very difficult to recreate in the liquid phase. Bias energy applied through different CVs results in various reactions, including the formation of BH_3, H_2, $BH_3(OH)$, NO_2, HCN, and HNC. Among all the CVs tested, the mechanistic study focuses on the WTMetaD trajectories of a single CV, the ∠BCN bond angle (Figure S1b), which is the most effective in promoting the chemical reaction of the $[EMIM]^+[CBH]^-$ + HNO_3 system. A Gaussian bias with a deposition rate of every 50 steps, a height of 0.5 kcal/mol, and a width of 0.1 rad is applied along this CV.

Figure 5 shows snapshots of representative trajectories for the formation of different products. Table 1 shows a list of the products obtained experimentally and in liquid-phase WTMetaD simulations. As stated earlier, proton transfers from the HNO_3 to a neighboring CBH anion in unbiased simulations. Hence, the simulations start with the $[H_3BCN\text{-}H]^+$ cation and $[NO_3]^-$ anion, and proton transfer among HNO_3 molecules is observed. Only 3 out of the 50 trajectories show that a proton from $[H_3BCN\text{-}H]$ is first abstracted by a neighboring NO_3^-. **int2'** then forms via a C−N tumbling, which is followed by a proton abstraction from the neighboring HNO_3 molecule to form HCN (Figure 5a). The bias energy barriers associated with these three trajectories are 25, 35, and 36 kcal/mol, which are significantly higher than the $[EMIM]^+/[CBH]^-$ + H_2O_2 reaction. In the majority of the trajectories (44 of 50 trajectories), the bias energy bends the ∠BCN bond angle, breaking the B−C bond and forming BH_3 and HNC molecules. In 6 of these trajectories, the N−OH bond in a neighboring HNO_3 molecule dissociates and then reacts with BH_3 to form BH_3OH^- and NO_2 (Figure 5b). Another interesting pathway (2 trajectories) forming HCN is shown in Figure 5c. Here, the CN group shuffles a proton between adjacent HNO_3 molecules. In another trajectory (Figure 5d), H_2 forms with all of the HNO_3 as spectators. Here, the rotation about ∠BCN forms HNC. The N−H bond dissociates simultaneously as the B−N bond forms. This results in a free H atom abstracting another H atom from the BH_3 group, forming H_2.

Table 1. List of Products Observed Experimentally and in Liquid-Phase Simulations[a]

system	experimental products	products observed in liquid phase simulations
$[EMIM]^+[CBH]^-$ + H_2O_2	HCN, BO_2, $\underline{H_2O}$, CO_2, CO, HNCO, CH_4, NH_3	$BH_2(OH)CN$, $\underline{H_2O}$
$[EMIM]^+[CBH]^-$ + HNO_3	N_2O, $\underline{HCN}$, $\underline{NO_2}$	$\underline{HCN}$, HNC, H_2, $BH_3(OH)^-$, $\underline{NO_2}$, BH_2NC

[a]If a species is observed in both experiments and simulations, it is underlined. It should be noted that simulations are stopped once the first reaction takes place and thus should be taken as the initial decomposition products. The experiments were not set to detect some of the species, e.g., H_2.

The bias energy profiles of 50 trajectories when the first reaction takes place are provided in Figure 4b. The barriers range between 11 and 40 kcal/mol with an average of 24.4 kcal/mol and a standard deviation of 6.9 kcal/mol. As stated in the Introduction, the lower bound of the barriers determines the system's reactivity. Therefore, the $[EMIM]^+[CBH]^-$ + HNO_3 system is considerably less reactive as compared to the $[EMIM]^+[CBH]^-$ + H_2O_2 system, whose lower bound is only 5 kcal/mol. This result supports the levitator experiment showing H_2O_2 is a more effective oxidizer than HNO_3 for $[EMIM]^+[CBH]^-$.[21,22,59]

To further investigate whether the $[EMIM]^+[CBH]^-$ + HNO_3 system follows a mechanism similar to that of the $[EMIM]^+[CBH]^-$ + H_2O_2 system, where $[CBH]^-$ hydroxylates to $H_2B(OH)CN^-$, an additional set of WTMetaD simulations is carried out. The CVs employed are shown in Figure S2. We use (1) the coordination number between boron in a randomly chosen CBH^- and all oxygen atoms in all the HNO_3 molecules, and (2) the coordination number of boron and three H-atoms in the -BH_3 group. By simultaneously enhancing the B−O coordination and weakening the B−H bonds, we explore potential hydroxylation pathways similar to the $[EMIM]^+[CBH]^-$ + H_2O_2 system. A Gaussian bias is deposited at every 50 frames with a height of 0.5 kcal/mol and a width of 0.1 for each CV. This set of CVs led to various reactions, including the formation of H_2, HCN, HNC, BH_3, $HNCH_2$, HNO_2, HBOH, H_2BONO_2, and $H_2B(ONO_2)$-OH^-. Snapshots from a representative trajectory are shown in the ESI (Figure S3). Although some of these products have

https://doi.org/10.1021/acs.jpcb.5c07210
J. Phys. Chem. B 2025, 129, 13258−13266

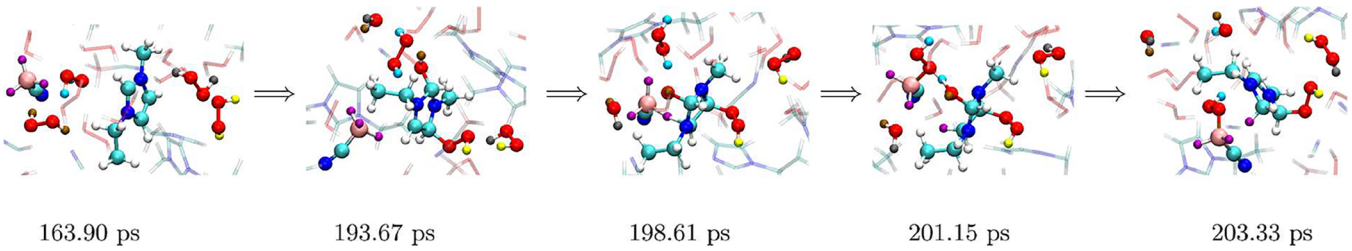

Figure 6. Snapshots of a trajectory showing the reaction between $EMIM^+$ and H_2O_2 followed by proton abstraction from the CBH anion.

been observed in the experiments,[59] the amount of the bias energy required ranges between 35 and 60 kcal/mol (Figure S4). These barriers are even higher than their counterpart from a single CV (e.g., ∠BCN bond angle); thus, this reaction pathway is considered unlikely to be the initial reaction.

Rate of the Reaction. Although it is difficult to prove that the reactions observed in WTMetaD simulations reflect how they will progress in reality, the key takeaways are that under disturbance (e.g., the bias energy), the $[EMIM]^+[CBH]^-$ + HNO_3 system is more stable than the $[EMIM]^+[CBH]^-$ + H_2O_2 system. As noted earlier, the WTMetaD simulations are terminated once the products/intermediates are formed, and the rates for the reactions can be assessed with methods like infrequent metadynamics (iMetaD).[60,61] In iMetaD, the acceleration factor for each simulation is approximated as a time-average over the simulation, and the rate constant is given as $k_0^* = {}^1/_{\langle \alpha_i t_i \rangle}$, where α_i and t_i are the acceleration factor and trajectory time of the i^{th} simulation, and the averaging is performed over all the independent trajectories. Running a set of trajectories in this case is essential because the barrier crossings are stochastic in nature, and results over a set of trajectories ensure statistical reliability.

As multiple sets of WTMetaD simulations are carried out for each system, the set possessing the lowest barrier in the bias energy is used for the rate constant assessment. Specifically, for the $[EMIM]^+[CBH]^-$ + H_2O_2, trajectories that are generated using the coordination number between all three hydrogens in -BH_3 and oxygens from all H_2O_2 molecules (CV1) and the coordination number between boron and three hydrogens in $-BH_3$ (CV2) and for the $[EMIM]^+[CBH]^-$ + HNO_3, trajectories generated using ∠BCN. The calculated rate constants are 9.6×10^{-16} fs^{-1} and 3.58×10^{-26} fs^{-1} for $[EMIM]^+[CBH]^-$ + H_2O_2 and $[EMIM]^+[CBH]^-$ + HNO_3, respectively. These results confirm that $[EMIM]^+[CBH]^-$ + H_2O_2 reacts significantly faster than does $[EMIM]^+[CBH]^-$ + HNO_3. To further assess the validity of the rate constant, an additional set of WTMetaD simulations for the $[EMIM]^+[CBH]^-$ + H_2O_2 system is carried out. A total of 50 trajectories are initiated with identical conditions as the previous set, but the Gaussian decomposition rate is now 10 times slower (i.e., every 500 steps). Since AIMD simulations on large systems (205 atoms in this case) are time-consuming, the simulation is extended to a maximum time of 250 ps or until a reaction takes place, whichever happens first. Out of 50, a total of 22 trajectories are reactive, with most following a pathway similar to that shown in Figure 3. In addition to the formation of $H_3B(OH)CN^-$ as mentioned earlier, formation of $H_3B(OOH)CN^-$ is also observed in a few trajectories. Interestingly, in one trajectory we observe a more complex reaction path involving the cation $EMIM^+$ − addition of −OH and -OOH on C1 and C4 of one of the $EMIM^+$ molecules, with O−O dissociation and proton-shuffle between multiple H_2O_2 molecules. This is followed by B−H dissociation and B−O bond formation in a CBH^- molecule. A rearrangement in reacted $EMIM^+$ gives a 3,4-addition product. Notably, this is the only trajectory in our whole study (including both fast and slow biasing rates of all sets of CVs) where an $EMIM^+$ molecule is directly involved in the reaction (Figure 6).

The rate constant of $[EMIM]^+[CBH]^-$ + H_2O_2 assessed from the new set of WTMetaD simulations (with a slower biasing rate) is 1.4×10^{-13} fs^{-1}. This value is estimated to be about 3 orders of magnitude larger than the previous estimate, as the system relaxes longer to dissipate the bias energy. Such a difference is consistent with previous iMetaD reaction rate assessments.[61] More importantly, the difference between the rate constants estimated from the original WTMetaD simulations and the slow-biasing WTMetaD simulations is well outside the range for the $[EMIM]^+[CBH]^-$ + HNO_3 reaction (3.58×10^{-26} fs^{-1}). This further confirms that H_2O_2 is a much more effective oxidizer for this specific ionic liquid. Here, we note that the WTMetaD simulations with slower biasing rates were not carried out for $[EMIM]^+[CBH]^-$ + HNO_3, as they are less reactive and require much longer simulation times. Developing a trustworthy machine-learning potential for such studies would significantly reduce the computational cost, but this is beyond the scope of the current manuscript.

CONCLUSION

In this work, we investigated the fundamental reaction mechanisms and kinetics of the $[EMIM]^+[CBH]^-$ ionic liquid with the oxidizers H_2O_2 and HNO_3 in liquid phases. No oxidation reactions were observed in the unbiased MD simulations. Thus, WTMetaD simulations were employed where the bias energy, applied along CVs, accelerates the reaction. A large number of different CVs were screened, and the analysis focused on the CVs that required the least amount of bias energy. We find that for the IL+H_2O_2 system, the barrier ranges from ∼5−20 kcal/mol, while for the IL+HNO_3 system, the barriers are significantly higher at ∼11−40 kcal/mol. These barrier differences between the two systems agree with the experiments, which found that rocket-grade H_2O_2 is a much more effective oxidizer for $[EMIM]^+[CBH]^-$. The ratio of the reaction rate constants was assessed with iMetaD and showed that the oxidation with H_2O_2 is about 10^{10} times faster than with HNO_3.

ASSOCIATED CONTENT

Supporting Information

The Supporting Information is available free of charge at https://pubs.acs.org/doi/10.1021/acs.jpcb.5c07210.

https://doi.org/10.1021/acs.jpcb.5c07210
J. Phys. Chem. B 2025, 129, 13258−13266

Collective variables for IL + H_2O_2 and IL + HNO_3, another set of collective variables for IL + HNO_3, bias energy deposition as a function of CV1′ and CV2′ and trajectory snapshots for IL + HNO_3, bias energy as a function of CV1′ and CV2′ of all reactive trajectories for IL + HNO_3 (PDF)

AUTHOR INFORMATION

Corresponding Author

Rui Sun − *Department of Chemistry, University of Hawaii, Honolulu, Hawaii 96822, United States;* orcid.org/0000-0003-0638-1353; Email: ruisun@hawaii.edu

Authors

Komal Yadav − *Department of Chemistry, University of Hawaii, Honolulu, Hawaii 96822, United States*

Ralf Kaiser − *Department of Chemistry, University of Hawaii, Honolulu, Hawaii 96822, United States;* orcid.org/0000-0002-7233-7206

Complete contact information is available at: https://pubs.acs.org/10.1021/acs.jpcb.5c07210

Notes

The authors declare no competing financial interest.

ACKNOWLEDGMENTS

This work was supported by the Air Force Office of Scientific Research (AFOSR) (FA9550-21-1-0377 and FA9550-25-1-0208). The authors acknowledge the Information and Technology Services (ITS) from the University of Hawai'i, Mānoa, and ACCESS for the computational resources that enabled the simulations.

REFERENCES

(1) Kang, H.; Jang, D.; Kwon, S. Demonstration of 500 N Scale Bipropellant Thruster Using Non-Toxic Hypergolic Fuel and Hydrogen Peroxide. *Aerosp Sci. Technol.* **2016**, *49*, 209−214.

(2) Ricker, S. C.; Brüggemann, D.; Freudenmann, D.; Ricker, R.; Schlechtriem, S. Protic Thiocyanate Ionic Liquids as Fuels for Hypergolic Bipropellants with Hydrogen Peroxide. *Fuel* **2022**, *328*, No. 125290.

(3) Nishihara, T.; Shiomi, A.; Kadotani, S.; Nokami, T.; Itoh, T. Remarkably Improved Stability and Enhanced Activity of a Burkholderia Cepacia Lipase by Coating with a Triazolium Alkyl-PEG Sulfate Ionic Liquid. *Green Chem.* **2017**, *19* (21), 5250−5256.

(4) Rogers, R. D.; Seddon, K. R. Ionic Liquids–Solvents of the Future? *Science (1979)* **2003**, *302* (5646), 792−793.

(5) Rothgery, E. F. Hydrazine and Its Derivatives. In *Kirk-Othmer Encyclopedia of Chemical Technology*; Wiley, 2004.

(6) Schneider, S.; Hawkins, T.; Rosander, M.; Vaghjiani, G.; Chambreau, S.; Drake, G. Ionic Liquids as Hypergolic Fuels. *Energy Fuels* **2008**, *22* (4), 2871−2872.

(7) Xue, H.; Gao, Y.; Twamley, B.; Shreeve, J. M. Energetic Azolium Azolate Salts. *Inorg. Chem.* **2005**, *44* (14), 5068−5072.

(8) Zeng, Z.; Twamley, B.; Shreeve, J. M. Structure and Properties of Substituted Imidazolium, Triazolium, and Tetrazolium Poly(1,2,4-Triazolyl)Borate Salts. *Organometallics* **2007**, *26* (7), 1782−1787.

(9) Reddy, G.; Song, J.; Mecchi, M. S.; Johnson, M. S. Genotoxicity Assessment of Two Hypergolic Energetic Propellant Compounds. *Mutation Research/Genetic Toxicology and Environmental Mutagenesis* **2010**, *700* (1−2), 26−31.

(10) Wang, S.; Thynell, S. T.; Chowdhury, A. Experimental Study on Hypergolic Interaction between *N,N,N′,N′* -Tetramethylethylenediamine and Nitric Acid. *Energy Fuels* **2010**, *24* (10), 5320−5330.

(11) Katritzky, A. R.; Rogers, J. W.; Witek, R. M.; Vakulenko, A. V.; Mohapatra, P. P.; Steel, P. J.; Damavarapu, R. Synthesis and Characterization of Blowing Agents and Hypergolics. *Journal of Energetic Materials* **2007**, *25* (2), 79−109.

(12) Zhang, Q.; Shreeve, J. M. Energetic Ionic Liquids as Explosives and Propellant Fuels: A New Journey of Ionic Liquid Chemistry. *Chem. Rev.* **2014**, *114* (20), 10527−10574.

(13) Zhang, Y.; Shreeve, J. M. Dicyanoborate-Based Ionic Liquids as Hypergolic Fluids. *Angew. Chem., Int. Ed.* **2011**, *50* (4), 935−937.

(14) Wang, K.; Zhang, Y.; Chand, D.; Parrish, D. A.; Shreeve, J. M. Boronium-Cation-Based Ionic Liquids as Hypergolic Fluids. *Chemistry − A. European Journal* **2012**, *18* (52), 16931−16937.

(15) Joo, Y.-H.; Gao, H.; Zhang, Y.; Shreeve, J. M. Inorganic or Organic Azide-Containing Hypergolic Ionic Liquids ⊥ ⊥ As Poster Published in 1st Korean International Symposium on High Energy Materials, Incheon, Korea, October 6−9, 2009. *Inorg. Chem.* **2010**, *49* (7), 3282−3288.

(16) McCrary, P. D.; Beasley, P. A.; Cojocaru, O. A.; Schneider, S.; Hawkins, T. W.; Perez, J. P. L.; McMahon, B. W.; Pfeil, M.; Boatz, J. A.; Anderson, S. L.; Son, S. F.; Rogers, R. D. Hypergolic Ionic Liquids to Mill, Suspend, and Ignite Boron Nanoparticles. *Chem. Commun.* **2012**, *48* (36), 4311.

(17) Chand, D.; Zhang, J.; Shreeve, J. M. Borohydride Ionic Liquids as Hypergolic Fuels: A Quest for Improved Stability. *Chemistry − A. European Journal* **2015**, *21* (38), 13297−13301.

(18) Gao, H.; Shreeve, J. M. Ionic Liquid Solubilized Boranes as Hypergolic Fluids. *J. Mater. Chem.* **2012**, *22* (22), 11022.

(19) He, L.; Tao, G.; Parrish, D. A.; Shreeve, J. M. Nitrocyanamide-Based Ionic Liquids and Their Potential Applications as Hypergolic Fuels. *Chemistry − A. European Journal* **2010**, *16* (19), 5736−5743.

(20) Watanabe, M.; Thomas, M. L.; Zhang, S.; Ueno, K.; Yasuda, T.; Dokko, K. Application of Ionic Liquids to Energy Storage and Conversion Materials and Devices. *Chem. Rev.* **2017**, *117* (10), 7190−7239.

(21) Biswas, S.; Fujioka, K.; Antonov, I.; Rizzo, G. L.; Chambreau, S. D.; Schneider, S.; Sun, R.; Kaiser, R. I. Hypergolic Ionic Liquids: To Be or Not to Be? *Chem. Sci.* **2024**, *15* (4), 1480−1487.

(22) Biswas, S.; Fujioka, K.; Paul, D.; Mcanally, M.; Rizzo, G. L.; Chambreau, S. D.; Schneider, S.; Sun, R.; Kaiser, R. I. Unraveling the Unusual Chemistry of the Hydrogen-Peroxide-Driven Hypergolic Ignition of a Cyanoborohydride Ionic Liquid as a Next-Generation Green Space Propellant. *J. Phys. Chem. Lett.* **2025**, *16* (8), 1831−1839.

(23) Ricker, S. C.; Freudenmann, D.; Schlechtriem, S. The Impact of Cation Structures on Hypergolicity of Thiocyanate Ionic Liquids with Hydrogen Peroxide. *Energy Fuels* **2021**, *35* (19), 16128−16133.

(24) Castaneda, D. A.; Natan, B. Hypergolic Ignition of Hydrogen Peroxide with Various Solid Fuels. *Fuel* **2022**, *316*, No. 123432.

(25) Jyoti, B. V. S.; Naseem, M. S.; Baek, S. W. Hypergolicity and Ignition Delay Study of Pure and Energized Ethanol Gel Fuel with Hydrogen Peroxide. *Combust. Flame* **2017**, *176*, 318−325.

(26) Kang, H.; Lee, E.; Kwon, S. Suppression of Hard Start for Nontoxic Hypergolic Thruster Using H_2O_2 Oxidizer. *J. Propuls Power* **2017**, *33* (5), 1111−1117.

(27) Mota, F. A. S.; Fei, L.; Tang, C.; Huang, Z.; Costa, F. S. Hypergolic Ignition Behaviors of Green Propellants with Hydrogen Peroxide: The TMEDA/DMEA System. *Fuel* **2023**, *336*, No. 127086.

(28) Bhosale, V. K.; Lee, K.; Yoon, H.; Kwon, S. Green Bipropellant: Performance Evaluation of Hypergolic Ionic Liquid-Biofuel with Hydrogen Peroxide. *Fuel* **2024**, *376*, No. 132688.

(29) Biswas, S.; McAnally, M.; Chambreau, S. D.; Schneider, S.; Sun, R.; Kaiser, R. I. Atmospheric Ignition Chemistry of Green Hypergolic Bipropellant 1-Ethyl-3-Methylimidazolium Cyanoborohydride − Hydrogen Peroxide in an Acoustic Levitator: Exploring a Potent Universal Propellant. *Chemistry − A. European Journal* **2025**, *31* (23), No. e202500593.

(30) Liu, J.; Zhou, W.; Chambreau, S. D.; Vaghjiani, G. L. Molecular Dynamics Simulations and Product Vibrational Spectral Analysis for the Reactions of NO_2 with 1-Ethyl-3-Methylimidazolium Dicyana-

mide ($EMIM^+DCA^-$), 1-Butyl-3-Methylimidazolium Dicyanamide ($BMIM^+DCA^-$), and 1-Allyl-3-Methylimidazolium Dicyanamide ($AMIM^+DCA^-$). *J. Phys. Chem. B* **2020**, *124* (21), 4303−4325.
(31) Elliott, G. M.; Boatz, J. A.; Gordon, M. S. The Degradation of the 2-Hydroxyethylhydrazinium Nitrate Ionic Liquid System. *J. Phys. Chem. A* **2024**, *128* (41), 8845−8855.
(32) Guo, R.; Jiang, S.; Qin, Y.; Lu, M.; Wang, P. Octahydrotriborate ($B_3H_8^-$) Based Hypergolic Ionic Liquids as Ultra-Fast Ignition Propellant Fuels with Superior Decomposition Efficiency. *Energetic Materials Frontiers* **2025**.
(33) Sun, R.; Siebert, M. R.; Xu, L.; Chambreau, S. D.; Vaghjiani, G. L.; Lischka, H.; Liu, J.; Hase, W. L. Direct Dynamics Simulation of the Activation and Dissociation of 1,5-Dinitrobiuret (HDNB). *J. Phys. Chem. A* **2014**, *118* (12), 2228−2236.
(34) Zhou, W.; Liu, J.; Chambreau, S. D.; Vaghjiani, G. L. Molecular Dynamics Simulations, Reaction Pathway and Mechanism Dissection, and Kinetics Modeling of the Nitric Acid Oxidation of Dicyanamide and Dicyanoborohydride Anions. *J. Phys. Chem. B* **2020**, *124* (49), 11175−11188.
(35) Liu, J.; Zhou, W.; Chambreau, S. D.; Vaghjiani, G. L. Computational Study of the Reaction of 1-Methyl-4-Amino-1,2,4-Triazolium Dicyanamide with NO_2: From Reaction Dynamics to Potential Surfaces, Kinetics and Spectroscopy. *J. Phys. Chem. B* **2019**, *123* (13), 2956−2970.
(36) Fujioka, K.; Kaiser, R. I.; Sun, R. Unsupervised Reaction Pathways Search for the Oxidation of Hypergolic Ionic Liquids: 1-Ethyl-3-Methylimidazolium Cyanoborohydride ($EMIM^+/CBH^-$) as a Case Study. *J. Phys. Chem. A* **2023**, *127* (4), 913−923.
(37) Martínez, L.; Andrade, R.; Birgin, E. G.; Martínez, J. M. PACKMOL: A Package for Building Initial Configurations for Molecular Dynamics Simulations. *J. Comput. Chem.* **2009**, *30* (13), 2157−2164.
(38) Wang, J.; Wolf, R. M.; Caldwell, J. W.; Kollman, P. A.; Case, D. A. Development and Testing of a General Amber Force Field. *J. Comput. Chem.* **2004**, *25* (9), 1157−1174.
(39) Kühne, T. D.; Iannuzzi, M.; Del Ben, M.; Rybkin, V. V.; Seewald, P.; Stein, F.; Laino, T.; Khaliullin, R. Z.; Schütt, O.; Schiffmann, F.; Golze, D.; Wilhelm, J.; Chulkov, S.; Bani-Hashemian, M. H.; Weber, V.; Borštnik, U.; Taillefumier, M.; Jakobovits, A. S.; Lazzaro, A.; Pabst, H.; Müller, T.; Schade, R.; Guidon, M.; Andermatt, S.; Holmberg, N.; Schenter, G. K.; Hehn, A.; Bussy, A.; Belleflamme, F.; Tabacchi, G.; Glöß, A.; Lass, M.; Bethune, I.; Mundy, C. J.; Plessl, C.; Watkins, M.; VandeVondele, J.; Krack, M.; Hutter, J. CP2K: An Electronic Structure and Molecular Dynamics Software Package - Quickstep: Efficient and Accurate Electronic Structure Calculations. *J. Chem. Phys.* **2020**, *152* (19), 194103.
(40) Martyna, G. J.; Tobias, D. J.; Klein, M. L. Constant Pressure Molecular Dynamics Algorithms. *J. Chem. Phys.* **1994**, *101* (5), 4177−4189.
(41) Bussi, G.; Donadio, D.; Parrinello, M. Canonical Sampling through Velocity Rescaling. *J. Chem. Phys.* **2007**, *126* (1), No. 014101.
(42) Becke, A. D. Density-Functional Exchange-Energy Approximation with Correct Asymptotic Behavior. *Phys. Rev. A (Coll Park)* **1988**, *38* (6), 3098−3100.
(43) Lee, C.; Yang, W.; Parr, R. G. Development of the Colle-Salvetti Correlation-Energy Formula into a Functional of the Electron Density. *Phys. Rev. B* **1988**, *37* (2), 785−789.
(44) Weigend, F.; Ahlrichs, R. Balanced Basis Sets of Split Valence, Triple Zeta Valence and Quadruple Zeta Valence Quality for H to Rn: Design and Assessment of Accuracy. *Phys. Chem. Chem. Phys.* **2005**, *7* (18), 3297−3305.
(45) Goedecker, S.; Teter, M.; Hutter, J. Separable Dual-Space Gaussian Pseudopotentials. *Phys. Rev. B* **1996**, *54* (3), 1703−1710.
(46) Wilhelm, J.; Hutter, J. Periodic GW Calculations in the Gaussian and Plane-Waves Scheme. *Phys. Rev. B* **2017**, *95* (23), No. 235123.
(47) Yoon, B.; Voth, G. A. Elucidating the Molecular Mechanism of CO_2 Capture by Amino Acid Ionic Liquids. *J. Am. Chem. Soc.* **2023**, *145* (29), 15663−15667.
(48) Yoon, B.; Chen, S.; Voth, G. A. On the Key Influence of Amino Acid Ionic Liquid Anions on CO_2 Capture. *J. Am. Chem. Soc.* **2024**, *146* (2), 1612−1618.
(49) Grimme, S.; Antony, J.; Ehrlich, S.; Krieg, H. A Consistent and Accurate Ab Initio Parametrization of Density Functional Dispersion Correction (DFT-D) for the 94 Elements H-Pu. *J. Chem. Phys.* **2010**, *132* (15), 154104.
(50) Bonomi, M.; Branduardi, D.; Bussi, G.; Camilloni, C.; Provasi, D.; Raiteri, P.; Donadio, D.; Marinelli, F.; Pietrucci, F.; Broglia, R. A.; Parrinello, M. PLUMED: A Portable Plugin for Free-Energy Calculations with Molecular Dynamics. *Comput. Phys. Commun.* **2009**, *180* (10), 1961−1972.
(51) Brotton, S. J.; Kaiser, R. I. Controlled Chemistry via Contactless Manipulation and Merging of Droplets in an Acoustic Levitator. *Anal. Chem.* **2020**, *92* (12), 8371−8377.
(52) Zhang, Q.; Yin, P.; Zhang, J.; Shreeve, J. M. Cyanoborohydride-Based Ionic Liquids as Green Aerospace Bipropellant Fuels. *Chemistry − A. European Journal* **2014**, *20* (23), 6909−6914.
(53) Schneider, S.; Hawkins, T.; Ahmed, Y.; Rosander, M.; Hudgens, L.; Mills, J. Green Bipropellants: Hydrogen-Rich Ionic Liquids That Are Hypergolic with Hydrogen Peroxide. *Angew. Chem., Int. Ed.* **2011**, *50* (26), 5886−5888.
(54) Hehre, W. J.; Ditchfield, R.; Pople, J. A. Self—Consistent Molecular Orbital Methods. XII. Further Extensions of Gaussian—Type Basis Sets for Use in Molecular Orbital Studies of Organic Molecules. *J. Chem. Phys.* **1972**, *56* (5), 2257−2261.
(55) Fukui, K. Formulation of the Reaction Coordinate. *J. Phys. Chem.* **1970**, *74* (23), 4161−4163.
(56) McCullagh, M.; Saunders, M. G.; Voth, G. A. Unraveling the Mystery of ATP Hydrolysis in Actin Filaments. *J. Am. Chem. Soc.* **2014**, *136* (37), 13053−13058.
(57) Sun, R.; Sode, O.; Dama, J. F.; Voth, G. A. Simulating Protein Mediated Hydrolysis of ATP and Other Nucleoside Triphosphates by Combining QM/MM Molecular Dynamics with Advances in Metadynamics. *J. Chem. Theory Comput* **2017**, *13* (5), 2332−2341.
(58) E, W.; Ren, W.; Vanden-Eijnden, E. Simplified and Improved String Method for Computing the Minimum Energy Paths in Barrier-Crossing Events. *J. Chem. Phys.* **2007**, *126* (16), 164103.
(59) Biswas, S.; Antonov, I.; Fujioka, K.; Rizzo, G. L.; Chambreau, S. D.; Schneider, S.; Sun, R.; Kaiser, R. I. Unraveling the Initial Steps of the Ignition Chemistry of the Hypergolic Ionic Liquid 1-Ethyl-3-Methylimidazolium Cyanoborohydride ([EMIM][CBH]) with Nitric Acid (HNO_3) Exploiting Chirped Pulse Triggered Droplet Merging. *Phys. Chem. Chem. Phys.* **2023**, *25* (9), 6602−6625.
(60) Voter, A. F. A Method for Accelerating the Molecular Dynamics Simulation of Infrequent Events. *J. Chem. Phys.* **1997**, *106* (11), 4665−4677.
(61) Mazzaferro, N.; Sasmal, S.; Cossio, P.; Hocky, G. M. Good Rates From Bad Coordinates: The Exponential Average Time-Dependent Rate Approach. *J. Chem. Theory Comput* **2024**, *20* (14), 5901−5912.

https://doi.org/10.1021/acs.jpcb.5c07210
J. Phys. Chem. B 2025, 129, 13258−13266